Pharmaceutical Research, Vol. 25, No. 6, June 2008 (© 2008)
DOI: 10.1007/s11095-008-9540-4

Research Paper

Formation of Stable Submicron Protein Particles by Thin Film Freezing

Joshua D. Engstrom,[1] Edwina S. Lai,[1] Baltej S. Ludher,[1] Bo Chen,[2] Thomas E. Milner,[2] Robert O. Williams III,[3] G. Barrie Kitto,[4] and Keith P. Johnston[1,5]

Received July 9, 2007; accepted January 17, 2008; published online February 21, 2008

Purpose. Highly stable, submicron lactate dehydrogenase (LDH) and lysozyme particles may be produced by thin film freezing (TFF) of aqueous solutions followed by lyophilization.
Methods. The LDH activity was determined by measuring the decrease in absorbance of NADH over time for the reaction of pyruvate to lactate. For lysozyme the particle morphology was determined by scanning electron microscopy (SEM) and compared with the specific surface area (BET) and the particle size, as measured by laser light scattering,
Results. Protein particles with an average diameter of 300 nm and 100% enzyme activity upon reconstitution (for LDH) were formed by TFF. Droplets of protein solutions, 3.6 mm in diameter, spread upon impact with 223 and 133 K metal surfaces to form cylindrical disks with thicknesses of 200–300 μm. Calculated cooling rates of the disks of 10^2 K/s were confirmed experimentally with infrared measurements.
Conclusions. The cooling rates of 10^2 K/s, intermediate to those in lyophilization (1 K/min) and spray freeze-drying (SFD) (10^6 K/s), were sufficiently fast to produce sub-micron protein particles with surface areas of 31–73 m^2/g, an order of magnitude higher than in lyophilization. In addition, the low surface area/volume ratio (32–45 cm^{-1}) of the gas–liquid interface led to minimal protein adsorption and denaturation relative to SFD.

KEY WORDS: gas-liquid interface; intermediate cooling rate; lactate dehydrogenase; sub-micron protein particle; thin film freezing.

INTRODUCTION

The ability to produce high surface area stable submicron and micron-sized protein particles would create new opportunities for depot, pulmonary, and transdermal delivery applications (1–9). In pulmonary delivery, high surface area porous particles with aerodynamic diameters between 1–3 μm may be deposited more efficiently in the deep lung compared to dense particles with similar aerodynamic diameters (1,8). In depot delivery, 300–500 nm submicron protein particles have been encapsulated uniformly into 10–50 μm diameter microspheres to achieve high protein loadings, while minimizing burst release (4,6,10,11).

Solid protein particles, stabilized by cryoprotectants including sugars, are often less susceptible to destabilization during storage (1,12–17) relative to proteins in solution. However, the formation of stable submicron protein particles with surface areas exceeding 10 m^2/g (4,18,19) is highly challenging, as the removal of water exposes protein molecules to large interfacial areas. Adsorption of protein at gas–liquid and ice–liquid interfaces often results in unfolding and aggregation (1,18–22). In lyophilization, the most common process for producing stable protein particles, particle growth during slow cooling (~1 K/min) limits the particle diameter to a minimum of a few microns with surface areas less than 1 m^2/g (21). The same limitation is true when drop freezing small aliquots (~20–50 μl) of protein solution into liquid nitrogen (23), freezing thick (>500 μm) films on a cooled shelf (24), and plunge freezing ultra-thin walled PCR tubes filled with protein solution into liquid nitrogen (23). In these techniques, the protein solution was cooled at rates between 1 to 10 K/s (23,24). Although the dried particles may be milled to form submicron particles, yields can be limited, size distributions are often broad, and the mechanical stress can lead to denaturation (1,21).

Submicron protein particles may be precipitated from aqueous solution by a variety of processes including spray-drying (11,21,22,25), supercritical CO_2-assisted aerosolization and bubble drying ($scCO_2$A-BD) (26), spray freeze-drying (SFD) (1,18,19,21), and spray freezing into liquids (SFL). In SFD, an aqueous solution containing dissolved protein is atomized into the cold gas above a cryogenic liquid (18,19,27–29). The 10 to 100 μm diameter atomized droplets travel through the cryogenic gas, where they may begin to

[1] Department of Chemical Engineering, The University of Texas at Austin, Austin, Texas 78712, USA.
[2] Department of Biomedical Engineering, The University of Texas at Austin, Austin, Texas 78712, USA.
[3] Division of Pharmaceutics, College of Pharmacy, The University of Texas at Austin, Austin, Texas 78712, USA.
[4] Department of Chemistry & Biochemistry, The University of Texas at Austin, Austin, Texas 78712, USA.
[5] To whom correspondence should be addressed. (e-mail: kpj@che.utexas.edu)

freeze (30), and freeze completely at a cooling rate of ~10^6 K/s after contacting the liquid cryogen. By systematically studying the effects of the separate spraying, freezing and drying steps in SFD, the large gas–liquid interface in the spraying step was shown to be the primary cause of protein aggregation for recombinant human interferon γ (rhIFN-γ) (19), lysozyme (31), and more recently lactate dehydrogenase (LDH) (32). The interfacially active protein adsorbs at this interface and subsequently unfolds and forms aggregates (1,11,18,19,21,33).

To minimize exposure to the gas–liquid interface, the spray nozzle was immersed under the surface of the cryogenic liquid in the SFL process. This modification resulted in less protein adsorption, denaturation and aggregation, and consequently, higher enzymatic activities than in SFD (31,32,34,35). The jet dimensions in SFL led to a cooling rate of ~10^3 K/s as a result of the Leidenfrost effect, in which evaporation of liquid nitrogen produced an insulating layer (32,36,37). The cooling rate was sufficiently fast to arrest the growth of submicron protein particles, without the need for ultra rapid cooling rates of 10^6 K/s in SFD (36). Thus, additional novel processes with cooling rates intermediate between those in SFD and lyophilization would be attractive for forming high surface area submicron particles, while mitigating the limitation of protein denaturation in SFD (31,32,36). Other freezing techniques such as plunge freezing into liquid cryogens, and thin film freezing (TFF), also known as cold metal block freezing, have been used to cool ~100 μm thick tissue samples at rates between 100 to 10,000 K/s (38–41), but protein solutions were not studied. The TFF process has been studied experimentally and modeled extensively for water and liquid metals (24,42–44), but not for pharmaceutical formulations.

In the TFF process (Fig. 1) liquid droplets fall from a given height and impact, spread, and freeze on a cooled solid substrate. Recently TFF was used to form high SSA powder (25–29 m^2/g) of the poorly water soluble drug danazol (45). Liquid droplets (~2–4 mm in diameter) were dispensed from a pipet above a cryogenically cooled metal surface (46,47). Upon impact, the droplets spread out into thin films (~100–400 μm) that froze on time scales of 70 to 1,000 ms, which corresponds to a cooling rate of ~10^2 K/s (42–44, 47–57). The cooling rates predicted with a 1D heat transfer model were in agreement with experimental measurements with an infrared (IR) camera (45). Since the cooling rates in TFF and SFL are comparable, TFF may be expected to be a desirable process for forming high surface area protein particles.

The primary objective of this study was to demonstrate submicron LDH and lysozyme particles (>10 m^2/g) with 100% enzyme activity may be formed with TFF followed by lyophilization. The cooling rate was designed to be sufficiently fast to arrest particle growth, whereas the relatively small liquid–gas interfacial surface area helps prevent protein adsorption, unfolding and aggregation. The results section presents dimensions of the thin films, stabilities (enzyme activity) of LDH powders after reconstitution, and morphologies of lysozyme particles determined by SEM and BET measurements of surface area. The discussion section gives cooling rates of the thin films determined by a 1D heat transfer model and IR measurement. A secondary objective was to compare the cooling rates, particle morphologies and protein stabilities for the intermediate cooling rate processes TFF and SFL, relative to the ultra-rapid cooling process, SFD, and in the slow process, lyophilization. A protein nucleation and growth mechanism is presented to explain the particle morphologies in terms of the cooling rates. In TFF, the much smaller area of the gas–liquid interface of the falling droplet and spread film relative to the atomized droplets in SFD will be shown to result in significantly less protein adsorption, and consequently, minimal denaturation and aggregation. Furthermore, the intermediate cooling rate (~10^2 K/s) will be shown to be sufficient to arrest particle growth to give surface areas >30 m^2/g.

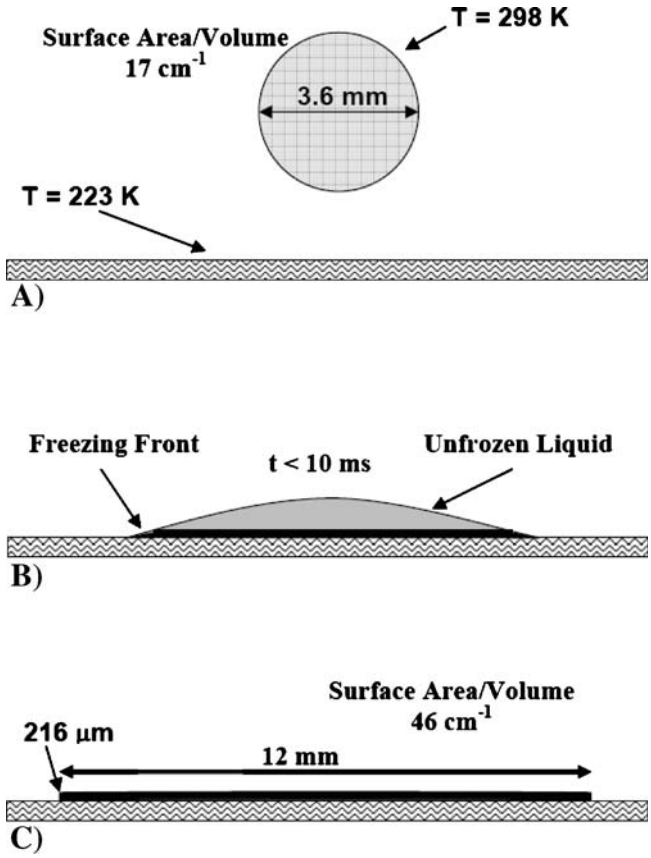

Fig. 1. Diagram of the thin film freezing process displaying the falling droplet (**A**), spreading after impact on the stainless steel surface (**B**), and during cooling and freezing as a thin film (**C**) (drawn to scale).

MATERIALS AND METHODS

Materials

Lysozyme was purchased from Sigma (St. Louis, MO) and L-LDH from porcine heart suspended in a 3.2 M ammonium sulfate solution from Roche Applied Science (Indianapolis, IN). Trehalose, NADH and pyruvate were purchased from Sigma (St. Louis, MO). The water was deionized by flowing distilled water through a series of 2× 7 l mixed bed vessels (Water and Power Technologies, Salt Lake City, UT) containing 60:40 anionic/cationic resin blends.

LDH Enzyme Preparation and Catalytic Activity Assay

The LDH enzyme preparation and catalytic activity assay used in this study is described in detail in a previous study (32). The LDH in ammonium sulfate was dialyzed against 10 mM KPO_4 buffer (pH 7.5) at 4°C for 3 h before use (58,59). LDH activities were measured for the reaction of pyruvate and NADH into lactate and NAD^+. Units of LDH activity (U) were calculated by measuring the decrease in absorbance of NADH at $\lambda = 340$ nm every 15 s for 1 min due to the conversion of NADH to NAD over time ($U = \Delta\mu$mol NADH/min) and then dividing by the mass (mg) of the LDH protein in solution to determine specific activity (U/mg). The stability of the LDH formulation in 30 mg/ml trehalose was measured over time. The LDH specific activity remained stable for an hour and then began to decrease. All experiments were performed in the time period where the LDH specific activity had not decayed. During this time period, the specific activity was defined as 100%.

Thin Film Freezing (TFF) Procedure

Aqueous protein solutions of LDH or lysozyme were passed at a flow rate of 4 ml/min either through a 17 gauge (1.1 mm ID, 1.5 mm OD) stainless steel syringe needle producing 3.6 mm diameter droplets or through 3.9 mm ID, 6.4 mm OD stainless steel tubing producing 5.6 mm diameter droplets. The droplets fell from a height of 10 cm above a rotating stainless steel drum 17 cm long and 12 cm in diameter. The cylindrical stainless steel drum was hollow with 0.7 cm thick walls and was filled with dry ice or liquid nitrogen on the inside. As a result of thermal conductivity through the steel, the resulting equilibrium drum surface temperatures were 223 K or 133 K for dry ice and liquid nitrogen, respectively. Before each run, the surface temperature of the drum was verified with a DiGi-Sense® Type K thermometer using a 45° angle surface probe thermocouple attachment (Eutech Instruments, Vernon Hills, IL). The drum rotated at approximately 12 rpm and was powered by a Heidolph RZR2041 mechanical overhead stirrer (ESSLAB, Essex, UK) connected to a speed reducer (Cat. No. GS6013G, Baldor, Fort Smith, AR). On impact the droplets deformed into thin films (Fig. 1) and froze. The frozen thin films were removed from the drum by a stainless steel blade mounted along the rotating drum surface. The frozen thin films then fell 5 cm into a 400 ml Pyrex® beaker filled with liquid nitrogen. Although the exposure of the cold drum to the atmosphere allowed a thin layer of ice to condense on the drum surface, the blade removed the ice immediately before the liquid droplets impacted the drum. For lysozyme, the frozen thin films in the 400 ml Pyrex® beakers were transferred directly to a −80°C freezer to evaporate excess liquid nitrogen. For LDH, the frozen thin films were transferred from the 400 ml Pyrex® beakers into 50 ml polypropylene tubes (Part No. UP2255, United Laboratory Plactics, St. Louis, MO) 2 cm in diameter and 16 cm in height using a spatula pre-cooled in liquid nitrogen.

Infrared Imaging of Cooling Thin Films

An InSb focal plane array (FPA) camera (Phoenix digital acquisition system (DAS) camera, Indigo Systems, Santa Barbara, CA) was positioned to acquire infrared images from above the cooling thin film on a flat plate. The FPA camera detected 3–5 μm radiation, and the images were acquired at 100 frames per second (10 ms/image). The dimensions of each frame were 256 pixels by 256 pixels (15×15 mm). The image spatial resolution was approximately 40 μm per pixel. Average intensity values were calculated using MATLAB® version 6 (20×20 pixel square within the center of the droplet) and plotted *versus* time to determine the time for the center of the thin film to reach thermal equilibrium with the plate.

Drying and Shelf Loading

A Virtis Advantage Lyophilizer (The Virtis Company, Inc., Gardiner, NY) was used to dry the frozen slurries. The 400 ml beakers containing frozen slurries of lysozyme and the 50 ml polypropylene tubes containing the frozen slurries of LDH were covered with a single layer Kim-wipe to prevent particles from exiting the tubes or beakers during drying. The beakers or tubes were filled to a depth of approximately 2 cm. Primary drying was carried out at −40°C for 36 h at 300 mTorr and secondary drying at 25°C for 24 h at 100 mTorr. A 12-h linear ramp of the shelf temperature from −40°C to +25°C was used at 100 mTorr.

LDH Reconstitution and Concentration Assay

Dried LDH powders were reconstituted with 1 ml of DI water and the enzyme assay was performed immediately. After all protein samples had been analyzed for enzymatic activity, the protein concentration was measured with the BCA (bicinchoninic acid) protein analysis kit (Sigma Chemical Company, St. Louis, MO). Once protein concentrations were determined, the specific activity from each measurement could be calculated. The activity of each LDH sample was normalized by the specific activity of the control measured immediately before the freezing process.

Transfer and Storage of Dried Powders

After the lyophilization cycle was complete, the lyophilizer was purged with nitrogen upon releasing the vacuum to reduce the exposure time of the protein powders to water vapor in the ambient air before transfer. The samples were then rapidly transferred to a dry box held at 14% RH, and the powders were transferred to 20 ml scintillation vials. The vials were then covered with 24 mm Teflon® Faced Silicone septa (Wheaton, Millville, NJ) which were held in place by open-top screw cap lids. Vials were purged with dry nitrogen for 2 min via a needle through the septa and an additional needle for the gas effluent.

Surface Area Measurement

Surface areas of dried powders were measured with a Quantachrome Nova 2000 (Quantachrome Corporation, Boynton Beach, FL) BET apparatus using nitrogen gas and the reproducibility in surface area was +1%. Dried powders were transferred to the glass BET sample cells in a dry box.

Samples were then degassed under vacuum for a minimum of 12 h. The Brunauer, Emmett, and Teller (BET) equation (60) was used to fit adsorption data of nitrogen at 77 K over a relative pressure range of 0.05–0.30. The samples were measured two times.

Residual Moisture Content

Aliquots of methanol were dispensed through the septum of the scintillation vials to form a suspension concentration of 10–100 mg/ml. Vials were then placed in a bath sonicator (Mettler Electronics, Anaheim, CA) for 5 min at maximum power to insure complete suspension of the powder. Moisture content was measured for a 200 µl aliquot with an Aquatest 8 Karl-Fischer Titrator (Photovolt Instruments, Indianapolis, IN). The moisture values were corrected with a 200 µl methanol blank control. All samples had a moisture content between 6–8% (*w*/*w*) after drying, comparable to values of 2–7% (*w*/*w*) for BSA prepared by SFD (18).

Particle Size Analysis

The size distribution of dried powders was measured by multiangle laser light scattering with a Malvern Mastersizer-S (Malvern Instruments, Ltd.,Worcestershire, UK). A mass of 30–100 mg of powder was suspended in 10 ml of acetonitrile and the suspension was then sonicated on ice for 1 min using a Branson Sonifier 450 (Branson Ultrasonics Corporation, Danbury, CT) with a 102 converter and tip operated in pulse mode at 35 W. Typical obscuration values ranged from 11% to 13%. Aliquots of the sonicated suspension were then dispensed into a 500 ml acetonitrile bath for analysis.

Scanning Electron Microscopy

SEM images were collected on a Hitachi Model S-4500 scanning electron microscope (Hitachi Ltd, Tokyo, Japan). The samples were prepared in a dry-box. Aluminum stages fitted with double adhesive carbon conducting tape were gently dipped into sample vials until covered by powder. Stages were then placed in septum capped vials and purged with nitrogen for transfer. To minimize the time samples were exposed to atmospheric moisture the stages were rapidly transferred to a Pelco Model 3 sputter-coater. A conductive gold layer was applied and the samples were then quickly transferred to the SEM. Total exposure to the atmosphere was less than 1 min.

RESULTS

The thin films formed from DI water droplets were characterized as a function of surface temperature and droplet diameter (Table I). The droplets spread on the cold metal surface and formed a cylindrical thin disk. The disk diameter decreased with a decrease in surface temperature from 223 K to 133 K and increased with an increase in falling droplet radius. By assuming the frozen thin films were cylindrical disks, the thicknesses of the thin films were calculated from the known volume of the liquid droplet and the measured disk diameter. The volumes of the falling droplets were determined by counting the number of droplets required to occupy 1 ml in a graduated cylinder. The average thin film thickness for the 223 and 133 K surfaces were 220 µm and 320 µm, respectively. The corresponding surface area/volume ratios for the top surfaces of the cylinders are also shown (Table I). The film thicknesses were essentially independent of the falling droplet diameter. For aqueous samples containing concentrations of lysozyme between 5 and 50 mg/ml or trehalose at 30 mg/ml, the droplet volumes, disk diameters, and thus film thicknesses did not change relative to pure water. The surface area/volume ratios for the 3.6 mm and 5.6 mm falling droplets in TFF were 17 and 11 cm^{-1}, respectively. As shown in Table I, upon impact the falling droplets spread into thin films with final surface area/volume ratios between 31 and 46 cm^{-1}. In a previous study (36) of SFD and SFL, the corresponding surface area/volume ratios were 6000 and 600 cm^{-1}, respectively, as determined for DI water and changed little with the presence of protein and excipient (Table I). Relative to these values, the much smaller surface area/volume ratio for TFF may be expected to lower the degree of protein destabilization from exposure to the gas–liquid interface.

The thin films were further characterized by determining the cooling rates from infrared measurements. The IR camera outputs intensity values with white indicating a high intensity and black a low intensity in relation to the amount of radiant energy E (energy density per unit time per unit wavelength) emitted from the droplet (45,61). The radiant energy E is related to the temperature of the object according to Planck's law:

$$E(\lambda, T) = (2\pi hc^2)/\{\lambda^5[\exp(hc/\lambda kT) - 1]\} \quad (1)$$

where λ is the wavelength, c is the speed of light, k is the Boltzmann constant, h is Planck's constant and T is the

Table I. Geometries of the Freezing Domains using DI Water for the SFD, SFL, and Thin Film Freezing Processes

			Thin Film from 3.6 mm Drop[b]		Thin Film from 5.6 mm Drop[c]	
	SFD[a]	SFL[a]	223 K[d]	133 K[d]	223 K[d]	133 K[d]
Droplet or thin film disk diameter (µm)	10	100	12,000	10,000	23,000	19,000
Film thickness (µm)	–	–	216	311	221	324
Droplet or thin film surface area to volume (cm^{-1})	6,000	600	46	32	45	31

[a] Values taken from Engstrom *et al.* (36)
[b] Surface Area to Volume of 3.6 mm droplet is 17 cm^{-1}
[c] Surface Area to Volume of 5.6 mm droplet is 11 cm^{-1}
[d] Temperatures of stainless steel plate

temperature in Kelvin (61). Therefore, the intensity output of the IR camera is related directly to the temperature.

For the thin film on the 223 K surface (Fig. 2A) the diameter of the film was 12 mm and the edge was uniform and smooth. As cooling progressed (Fig. 2A) a cooling front moved radially inward from the edge of the film toward the center. The center of the film reached thermal equilibrium in 1.6 s (Figs. 2A and 3). For the thin film on the 133 K surface (Fig. 2B), the diameter was 10 mm (Fig. 2B) and dark jagged "fingers" were observed at the edge, indicating the coldest domains. The cooling front moved radially inward from the edge to the center at first. Next the center turned black, and an annular region between the center and the outer jagged edge remained gray. The cooling front then reversed direction by moving from the center toward the edge of the film.

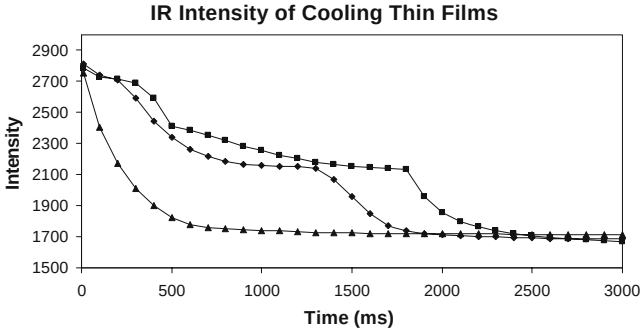

Fig. 3. IR intensity *versus* time for an aqueous thin film on stainless steel surface at 223 K measured at the center of the film (*filled diamonds*) and near the edge of the film (*filled triangles*) and at 133 K at the center of the film (*filled squares*).

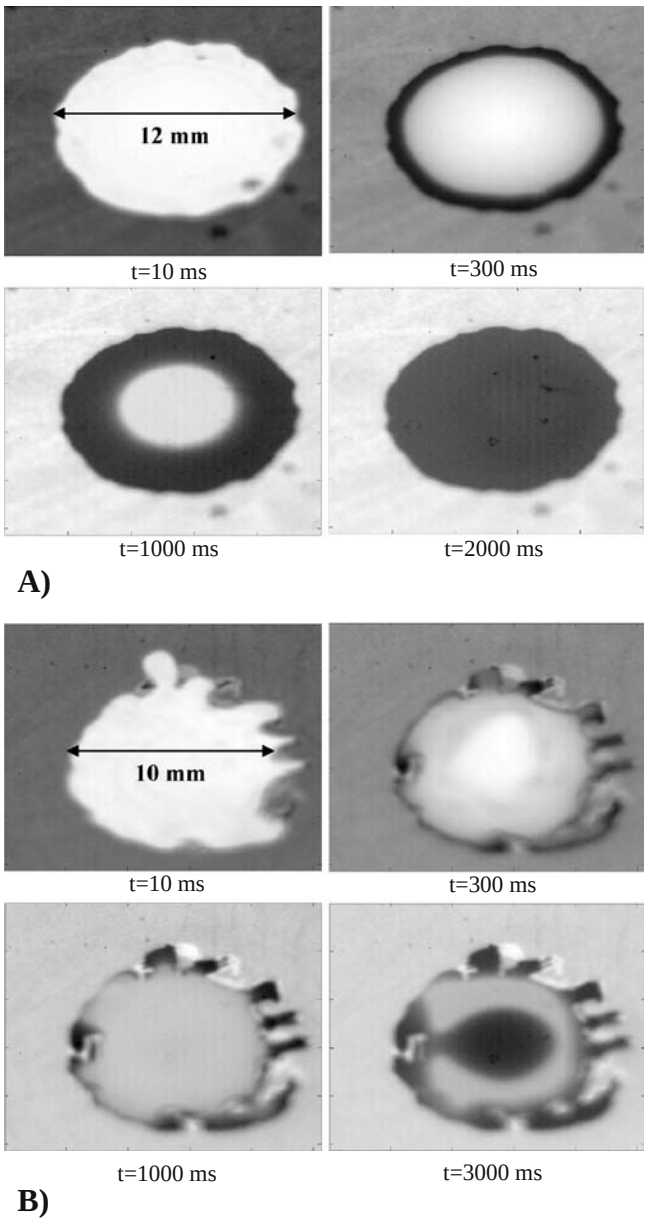

Fig. 2. IR photographs of an aqueous droplet impinging and freezing on a stainless steel surface at 223 K (**A**) and 133 K (**B**).

The center of the film reached thermal equilibrium a little more slowly, in about 3 s (Fig. 3), relative to 223 K. In each case at the center of the film, a plateau was observed and then an abrupt final decay to thermal equilibrium.

The LDH activities for an aqueous formulation of 0.25 mg/ml LDH with 30 mg/ml trehalose frozen by lyophilization, SFL (32), and TFF were extremely high (Table II) and not significantly different ($p<0.05$) according to a Student's t test. Compared to the SFD process for three droplet sizes, the LDH activities for each TFF condition were significantly higher ($p<0.05$). The very high LDH activities were maintained in the TFF process throughout the serial stresses of droplet falling and spreading, freezing, drying, and reconstitution.

Given the high enzyme activities for LDH particles formed by TFF, the other key goal was to demonstrate particle morphologies with submicron particle sizes and large particle surface areas (Table III). In the case of LDH, the ratio of LDH:trehalose was 1:120 by mass. As discussed previously (32,36), the particle surface area for trehalose decreased upon exposure to atmospheric moisture which lowers the T_g sharply. (This limitation may be overcome in the future with the use of lyostoppers to seal the vials from moisture.) Thus, we chose lysozyme as a model protein to investigate powder morphology instead of LDH:trehalose. Lysozyme samples obtained and transferred at room temperature had moisture contents between 6–8% as determined by Karl Fischer titration. For moisture contents between 7–8% by weight, the T_g remained high, between 50–60°C (62). Therefore the loss in lysozyme SSA during transfer may be expected to be negligible. For most cases, the SSA values were similar ranging between 30 and 55 m^2/g. For 5 mg/ml lysozyme, the thinner films at 223 K produced a significantly higher SSA of 73 m^2/g relative to the films at 133 K. In a previous study (36), 5 and 50 mg/ml lysozyme solutions processed by SFL had measured powder SSAs of 114 m^2/g and 34 m^2/g, respectively, similar to the values produced by TFF (36). The lyophilization protocols were the same in both studies. Although the SSA of 126 m^2/g for SFD was about twofold larger than for TFF, the enzyme activity was much smaller, as shown in Table II.

As shown in Table III, the volume percentage of submicron particles, determined by laser light scattering,

Table II. Activities for 0.25 mg/ml LDH, 30 mg/ml Trehalose Formulations Frozen by Various Techniques in pH 7.5, 10 mM KPO_4 Buffer in Replicates of 3

	Percent Activity	
Freezing process	223 K	133 K
Thin film (3.6 mm drop)	100±3.9	104±12.0
Thin film (5.6 mm drop)	97±9.5	100±8.4
SFL[a,d]	98±5.3	
SFD-130 μm[a]	85±8.2	
SFD-40 μm[a,e]	74±6.7	
SFD-10 μm[a,d]	80±5.4	
Falling droplet (3.6 mm)[c]	98±2.1	
Spray into air (10 μm)[a,b,c]	85±7.7	
Lyophilization	99±2.1	

[a] Values taken from Engstrom *et al.* (32)
[b] 100 mg/ml trehalose used in LDH formulation
[c] The droplets were not frozen in these two controls
[d] Replicate of 4
[e] Replicate of 5

after sonication of the 5 mg/ml lysozyme formulation prepared by TFF at 223 K, ranged from 88 to 92%. The similarity in these two values was expected since the nearly identical thin film thicknesses would be expected to produce similar cooling rates. These values were similar to those for the SFL powders (36). For TFF, the protein powders were friable and could be broken up readily into submicron particles with minimal sonication. As shown in Fig. 4 the D (v,50) was 300 nm. In contrast, the same 5 mg/ml lysozyme formulation prepared by lyophilization had a very low fraction of 7% submicron particles (Fig. 4 and Table III). As the lysozyme feed concentration was raised to 50 mg/ml the submicron fraction decreased to 66 and 62% on the 223 K and 133 K surfaces, respectively (Table III). The corresponding value for SFL was lower (48%), whereas for SFD it was higher (74%) (36). For the SFD powders, the D (v,50) was approximately 300 nm (36). A second peak with micron-sized particles was present for the 50 mg/ml lysozyme solution prepared by SFL and TFF as shown in Table III. However, 50 mg/ml is an unusually high protein concentration and TFF would ordinarily be applied to concentrations on the order of 5 mg/ml, where the second larger peak is not present (Fig. 4).

Selected SEM images from the results in Table III are shown in Fig. 5 and 6. For 5 mg/ml lysozyme, fine 50 nm primary particles were produced by TFF at 223 K (Fig. 5A), comparable to those produced by SFL (36) (Fig. 5C). At 133 K, larger 50–100 nm diameter particles were mixed with rods 50–100 nm in diameter and more than 500 nm long (Fig. 5B). The larger particles sizes shown in Fig. 5B compared to Fig. 5A are consistent with the slightly lower content of submicron particles measured by light scattering in Table III.

For 50 mg/ml lysozyme solutions and a surface temperature of 223 K (Fig. 6A), large sheets were observed with features between 1 and 2 μm. Similar features were observed for SFL (36). In contrast, a fine web with 100 nm features were produced by SFD (36) (Fig. 6C) consistent with the smaller particle sizes measured by light scattering in Table III. The larger features observed in the TFF and SFL processes for 50 mg/ml *versus* 5 mg/ml solutions are consistent with the particle size distributions measured by light scattering. The similarity of the particle morphologies for the powders prepared by the SFL and TFF processes at both the 5 and 50 mg/ml concentrations will now be examined in terms of cooling rates.

DISCUSSION

Modeling the Cooling Rate of Thin Films

Droplet spreading to form thin films of liquid metal and water droplets has been described in term of the Weber number, $We=\rho V^2 D/\gamma$ (inertial to interfacial forces) where ρ is the liquid droplet density, V is the impact velocity, D is the droplet diameter, and γ is the droplet interfacial tension in air. For We >30 immediately before impacting the cooled solid substrate (42,48–50,56,63) the droplets deformed into cylindrical thin films before freezing. For the low We<1 regime, impacting droplets froze as spherical domes with minimal droplet spreading (49,64). For the falling liquid droplets in this study γ(air–water)=72 mN/m and $V=(2gH)^{1/2}$ (65) where the falling height, H, of the droplet was 10 cm, resulting in V=1.4 m/s. The

Table III. Specific Surface Area Measurements and Particle Size Distributions for Lysozyme Powders Formed by Thin Film Freezing, SFL, and SFD

Freeze Process	Lysozyme Concentration (mg/ml)	SSA (m^2/g)		Size (μm)	
		223 K[a]	133 K[a]	223 K[a]	133 K[a]
Thin film (3.6 mm drop)	5	73±0.8	45±0.4	0.050–1.0 (88%) 1.0–10 (12%)	0.050–1.0 (81%) 1.0–12 (19%)
Thin film (5.6 mm drop)	5	–	–	0.050–1.0 (92%) 1.0–12 (8%)	0.050–1.0 (84%) 1.0–10 (16%)
Thin film (3.6 mm drop)	50	31±0.1	55±0.4	0.050–1.0 (66%) 1.0–30 (34%)	0.050–1.0 (62%) 1.0–30 (38%)
SFL[b]	5	114±11		0.050–1.0 (85%) 2.0–10 (15%)	
SFL[b]	50	34±2		0.050–1.0 (48%) 4.0–12 (52%)	
SFD-10 μm[b]	50	126±5		0.050–1.0 (74%) 1.0–10 (26%)	
Lyophilization	5	4.4±0.2		0.05–1.0 (7%) 4.8–120 (93%)	

[a] Temperatures of stainless steel plate
[b] Values taken from Engstrom *et al.* (36)

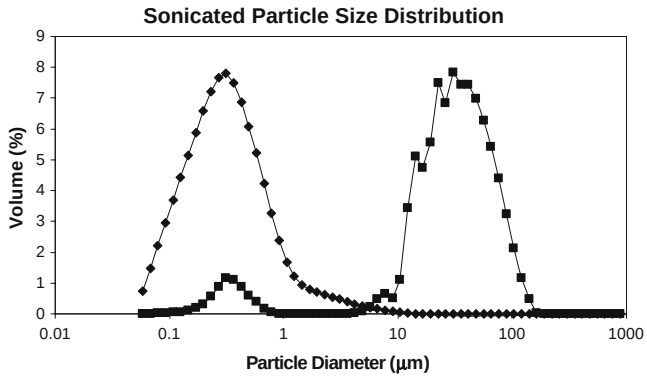

Fig. 4. Laser light scattering of particles formed by thin film freezing (*filled diamonds*) and lyophilization (*filled squares*) of 5 mg/ml lysozyme solutions followed by sonication.

observed formation of thin cylindrical disks was consistent with this We of 97, but when H was reduced to less than 1 cm (We= 9.8) the impacting water droplets froze as spherical domes that were only 4 mm in diameter.

Previously it was shown with IR imaging studies of thin films formed with acetonitrile and t-butanol that droplet spreading occurred within the first 10 ms interval indicating that the droplet spreading time was much less than the freezing time (45) (the same behavior was observed in Fig. 2 for water). The prediction of the cooling rate of the film with a simplified analytical heat transfer model was in good agreement with experimental IR data (45). Herein, this approach is extended to thin film freezing of water droplets.

Briefly, based on the experimental results observed above, the model assumes that the droplet spreads to form a cylindrical film on a much shorter time scale than heat transfer. Since the height (thickness) of the thin film is on the order of 200–400 µm, relative to a much larger diameter of 10–12 mm, radial heat transfer is neglected. The thermal diffusivity, $a=k/\rho*C_p$, where k is the thermal conductivity, ρ is the density, and C_p is the heat capacity, is treated as constant over the entire temperature range. For the case of freezing water the thermal diffusivities of water and ice are averaged. One-dimensional heat transfer for a

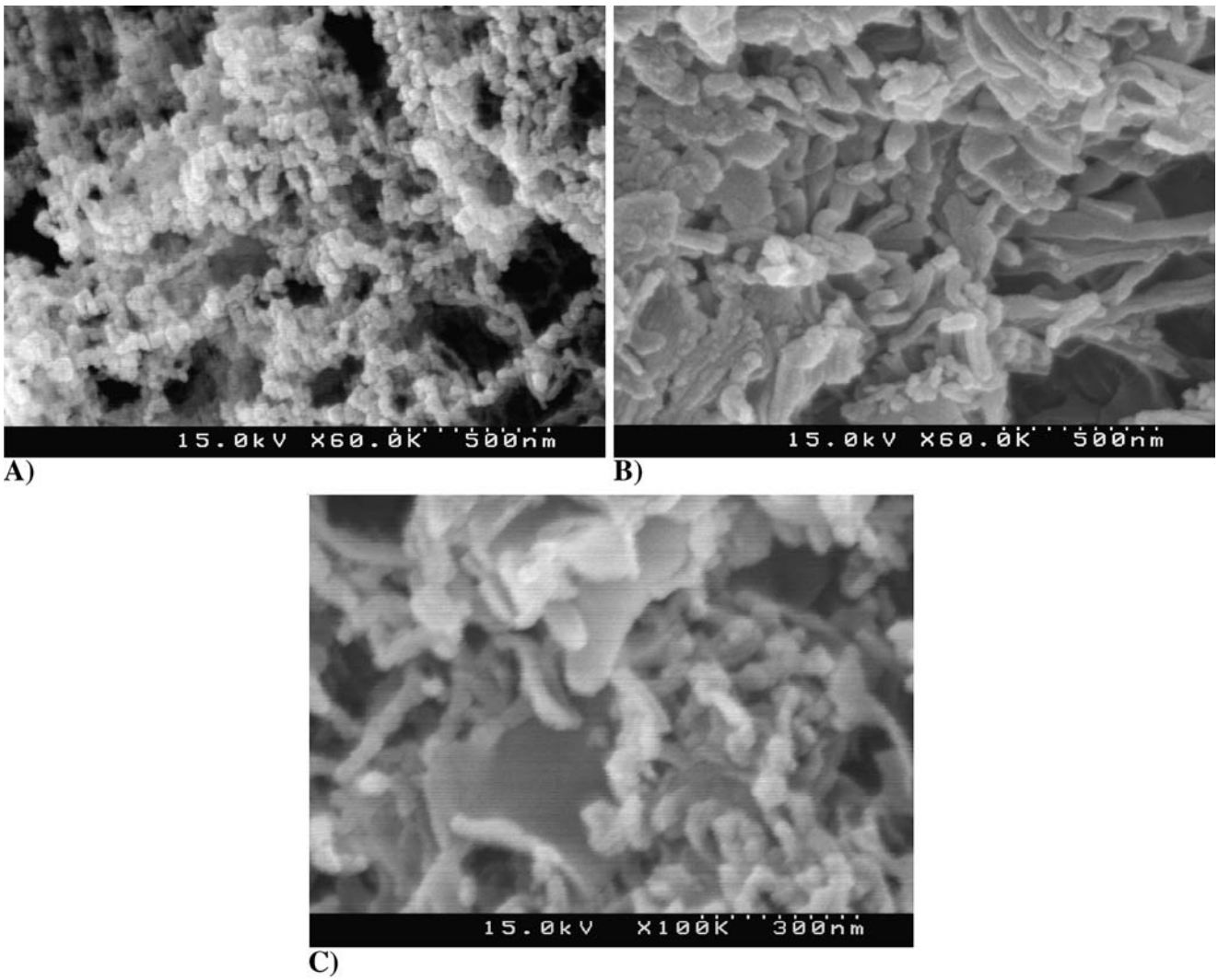

Fig. 5. SEM of particles from 5 mg/ml lysozyme solutions processed by thin film freezing at surface temperatures of 223 K (**A**) and 133 K (**B**), and SFL-LN2 (**C**).

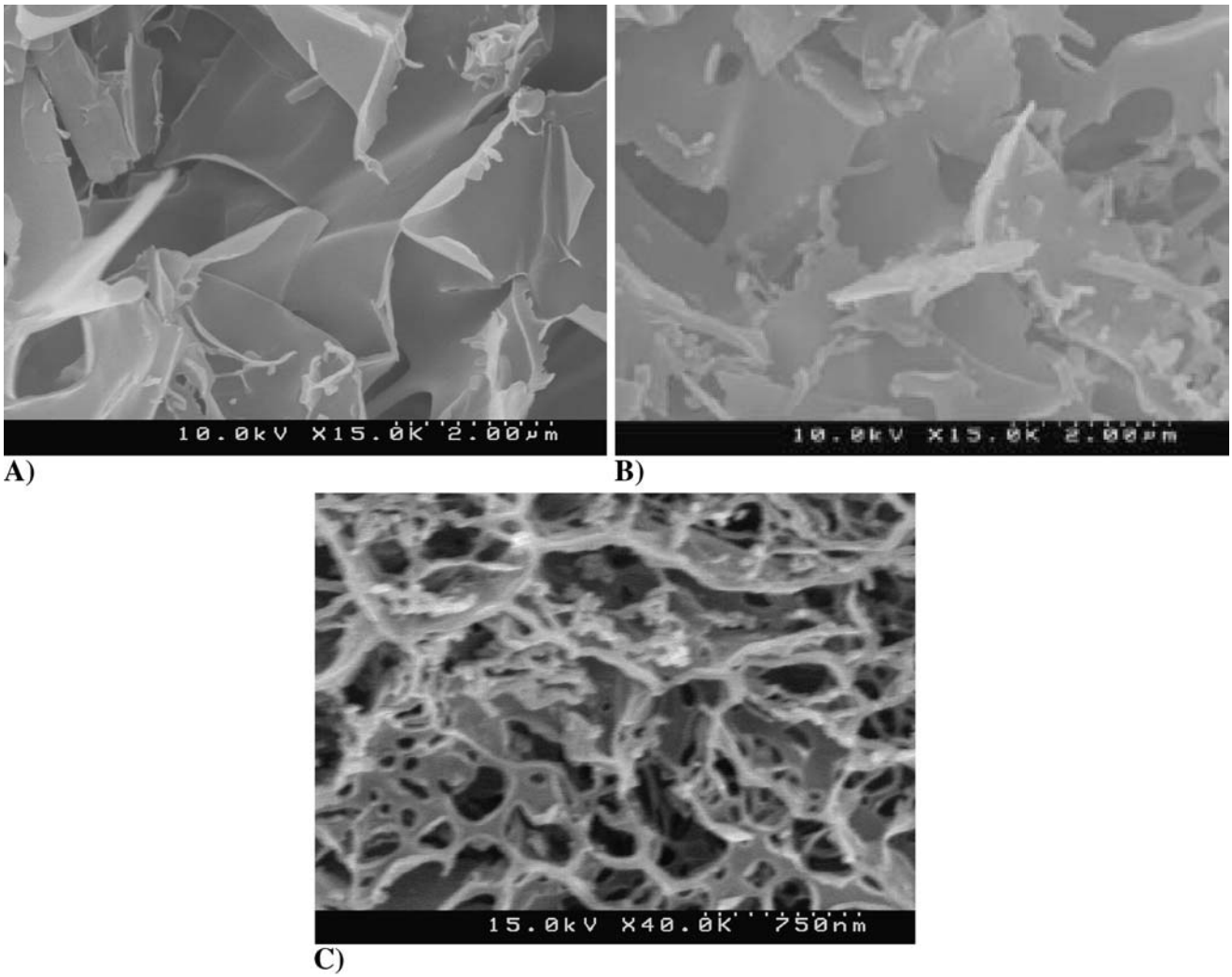

Fig. 6. SEM of particles from 50 mg/ml lysozyme solution processed by thin film freezing at a surface temperature of 223 K (**A**), SFL-LN2 (**B**), and SFD-10 μm into LN2 (**C**).

finite slab with an insulating boundary condition on the top surface of the thin film (air) and a constant temperature boundary condition on the bottom is described by (66):

$$T(x,t) = T_p + \frac{2}{L}\sum_{n=0}^{\infty} e^{-\alpha(2n+1)^2\pi^2 t/4L^2} \cos\frac{(2n+1)\pi x}{2L}\left\{\frac{2L(-1)^{n+1}T_p}{(2n+1)\pi} + \int_0^L T_i \frac{\cos(2n+1)\pi x'}{2L}dx'\right\} \quad (2)$$

where x is the distance from the top of the spread droplet, T is the temperature in the film, T_p is the plate temperature in contact with the bottom thin film surface, and L is the film thickness.

The calculated temperature profiles from Eq. 2 are shown in Fig. 7 and the calculated cooling rates and times are shown in Table IV. The cooling time was defined as the time for the temperature of the top surface of the film, T(0,t), to decrease from room temperature (25°C) to a value 5% greater than that of the metal surface. The cooling rate (K/s) was then determined by dividing the temperature difference at the top of the film by the cooling time. As shown in Fig. 7A and Table IV the predicted time to cool the top surface of the 220 μm thick thin film on the 223 K surface is 2.0×10^2 ms (cooling rate of 3.9×10^2 K/s). The calculated cooling rate is an order of magnitude less than for SFL (7.2×10^3 K/s) and 4 orders of magnitude less than for SFD (3.8×10^6 K/s). The much smaller cooling rates in TFF *versus* SFD may be explained by a 100-fold smaller surface area/volume ratio and a film thickness on the order of 20–30 times larger than the droplet radius in SFD (Table I).

The particle morphologies shown in Fig. 5 and particle SSAs in Table III were similar for freezing on the 223 K and 133 K surfaces, as a consequence of the rapid cooling in each case. However, for completeness, we discuss small differences in the cooling behavior for these two surface temperatures (Fig. 2) in the supplemental section.

The experimental cooling times to reach thermal equilibrium were longer by a factor of 3–4 compared to the modeled cooling times (Table IV). This difference is small compared to difference in orders of magnitude relative to other processes such as SFL and lyophilization. The difference may be the result of uncertainty in the calibration of the

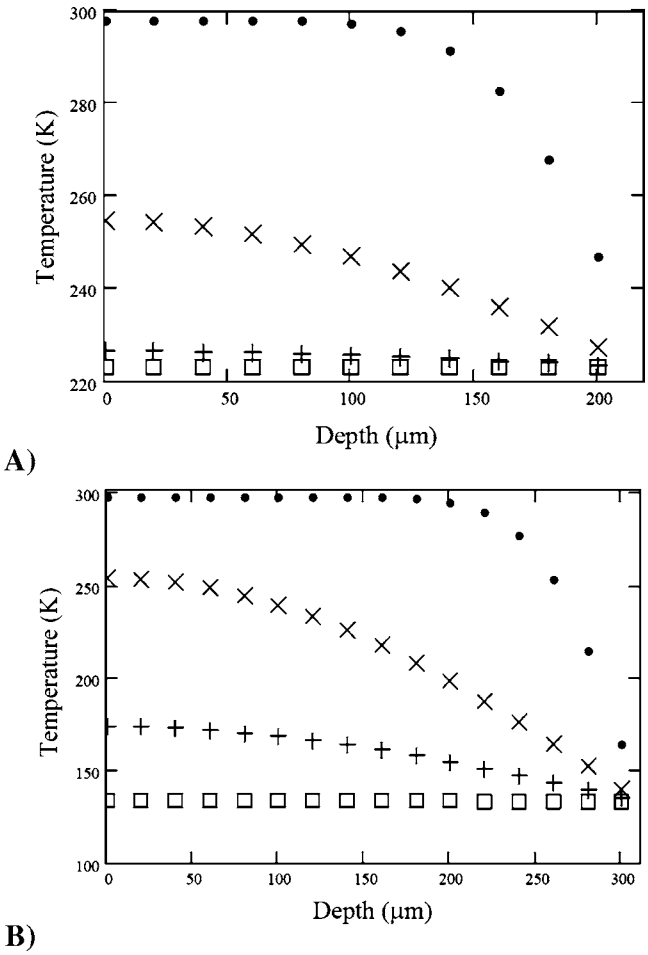

Fig. 7. Temperature *versus* depth profiles of thin aqueous films cooled on a surface at 223 K (**A**) for a 220 μm thin film and 133 K (**B**) for a 320 μm thin film. Time profiles were calculated after droplet impact at t=10 ms (*filled circles*), 100 ms (*cross marks*), 300 ms (*plus signs*), and 1000 ms (*open squares*).

temperature measurement, differences in definitions of the final temperature for the model and IR camera, and the release of the heat of fusion of water which was not factored into the model. For extremely rapid cooling rates of water, the water may form a glass with limited crystallization (67). As shown by experiment and calculation a cooling rate of 10^6 K/s is necessary to vitrify water (67–70). The 10^2 K/s cooling rate observed experimentally in TFF indicates that the latent heat of fusion may have been significant.

Nucleation and Growth Mechanisms *versus* Cooling Rate

To place the TFF results in perspective, it is instructive to consider the boundary conditions of extremely rapid vitrification/freezing in SFD and slow freezing in lyophilization. Previously, the morphologies of lysozyme powders prepared by SFL and SFD were shown to be similar for dilute 5 mg/ml lysozyme solutions. The SSAs were >100 m^2/g for 50–100 nm spherical primary particles, despite a cooling rate of 10^3 K/s for SFL *versus* 10^6 K/s for SFD, as shown in Table IV (36).

The freezing mechanism involves many simultaneous changes in the properties of the unfrozen solution. As the water freezes, it changes concentrations, pH, ionic strength, viscosity, diffusion coefficients, collisions between nucleated particles and geometric size and shape of the unfrozen solution. The growth rate of the protein particles depends upon all of these factors, such that it would be challenging to develop a model for the final particle size. The thin liquid channels between the frozen water domains reduce the number of collisions between protein (sugar) particles and thus inhibit growth by coagulation, as shown in Fig. 8. Furthermore, the viscosity of the thin channels increases rapidly to arrest particle growth and the channel fully freezes. Furthermore, the sugar in the water raises the viscosity over that of pure water. For the case of slow cooling in lyophilization, the very low degree of supercooling creates relatively few nucleated ice domains compared to the rapid cooling processes, leaving thick channels of liquid solution between these domains (Fig. 8). For a cooling rate of 1 K/min, as for the case of slowly cooling a 5 mg/ml solution in a −20°C freezer, the lyophilized particle sizes were on the order of 30–100 μm. In these thick channels, the protein particles have sufficient time to aggregate and grow forming large particles before the channels are fully frozen. Although it is theoretically possible to mitigate this particle growth partially by reducing the protein solution concentration significantly below 1 mg/ml, such low protein concentrations can lead to excessive lyophilization requirements (21).

In SFD, various studies found that exposure of the protein to the gas–liquid interface has a larger effect on protein stability than to the ice–liquid or glassy water–liquid interface (19,31,32). It is unclear whether ice–liquid *versus* glassy water–liquid interfaces have different effects on protein stabilities (19,20,71). As described by previous studies (68,69), cooling rates on the order of 10^6 K/s are needed to vitrify water, but the cooling rate necessary for vitrification can be lowered in the presence of sugar in solution (67,70). For the slower cooling rates observed in TFF (10^2 K/s) relative to SFD, it is likely that ice particle domains instead of vitrified water domains are formed. The LDH activities were on the order of 100% for TFF. Thus, our results do not suggest that the ice-liquid interface has a detrimental effect on protein stability.

For the 5 mg/ml lysozyme formulation at 223 K, the SSA was quite large, although modestly smaller than for SFD, and the particle sizes after sonication were similar to those of both

Table IV. Calculated Cooling Rates, Cooling Times, and Exposure Time to the Gas–liquid Interface for SFD, SFL, and TFF

	SFD[a]	SFL[a]	Thin Film from 3.6 mm Drop 223 K	Thin Film from 3.6 mm Drop 133 K
Cooling rate (K/s)	3.8×10^6	7.2×10^3	3.9×10^2	2.0×10^2
Cooling time (ms)	0.033	17	2.0×10^2	6.2×10^2
Droplet gas–liquid exposure time (ms)	10–1,000	2	~1,000	~1,000

The droplet dimensions are given in Table I
[a] Values taken from Engstrom *et al.* (36)

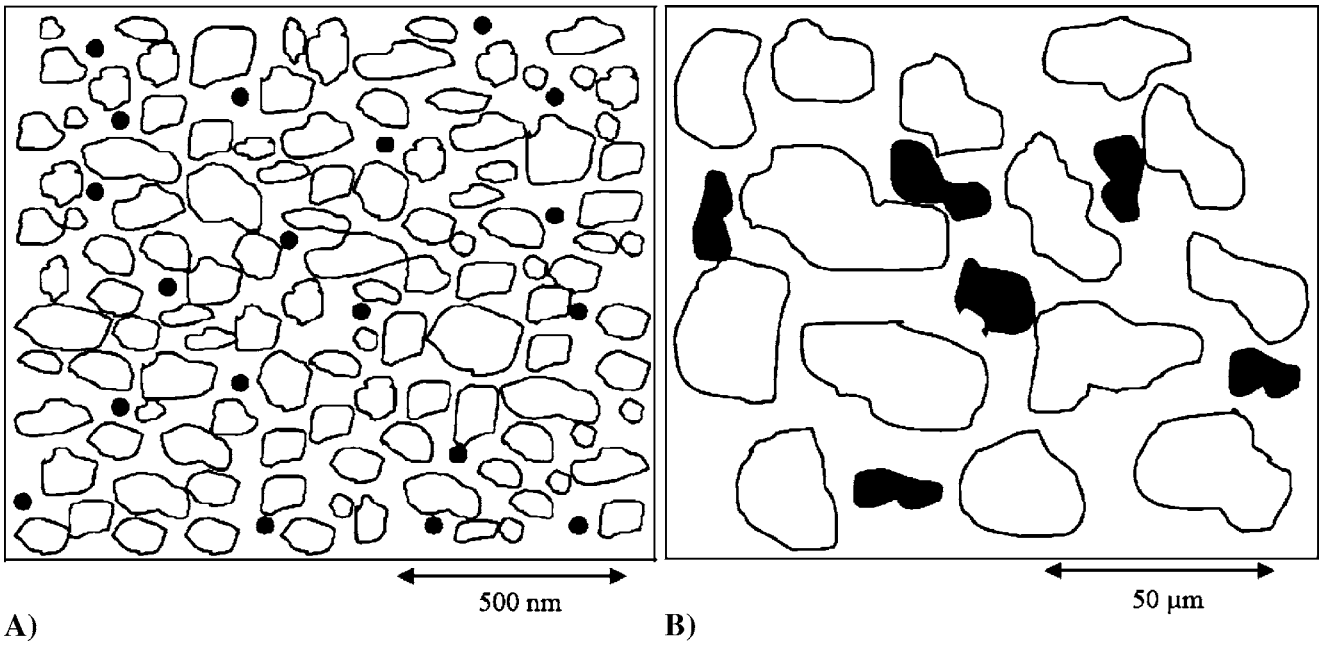

Fig. 8. Nucleation and growth of protein particle in unfrozen channels between glassy frozen water domains with high supercooling in the thin film freezing, SFL, and SFD processes(**A**), and with low supercooling in shelf lyophilization (**B**). Ice particles are represented as *white domains* and solute precipitate as *solid black dots* or regions.

SFL and SFD (Table III). The lower cooling rate in TFF (10^2 K/s) compared to SFD (10^6 K/s) and SFL (10^3 K/s) was still sufficient to produce rapid nucleation and to prevent significant particle growth during freezing. However, for TFF, the size of the unfrozen channels was sufficiently thin and the increase in the viscosity of the unfrozen solution sufficiently fast to achieve similar particle sizes and morphologies as for the moderately faster process, SFL and much faster process, SFD. Thus, the extremely rapidly cooling rates in SFD were much faster than necessary to form submicron protein particles. A similar conclusion was reached in the comparison of SFL and SFD (32).

For 50 mg/ml highly concentrated solutions the larger volume fraction of vitrified solute domains in the unfrozen water channels lead to a greater collision frequency and increased particle growth (36). As observed previously (36), the slower cooling rate in SFL compared to SFD leads to greater particle growth before the large unfrozen liquid channels vitrify, leading to larger protein particles and lower powder SSAs (36). As shown in Table III, the SSAs were similar for TFF and SFL. For these highly concentrated solutions, the larger particles formed in TFF (and SFL) *versus* SFD results from more time for growth in the thicker unfrozen channels. This limitation is typically not encountered in rapid freezing processes, as most previous studies examined much lower concentrations on the order of 5 mg/ml.

Minimization of Gas–liquid Interface in TFF Process

The LDH stabilities were essentially 100% after TFF indicating that none of the steps, droplet falling, spreading and freezing, and drying caused a measurable loss in enzyme activity. From previous calculations (32) it was shown that the exposure of the atomized droplets to the gas–liquid interface was an order of magnitude less in the SFL process (600 cm^{-1}) relative to SFD (6000 cm^{-1}) (19). This larger exposure to the gas–liquid interface resulted in lower LDH activities in SFD and in spray drying (32). In TFF the surface area/volume ratio of the gas–liquid interface of TFF (46 cm^{-1}) was 2 orders of magnitude lower than in SFD, leading to far less protein adsorption and aggregation (Table IV). As shown in Fig. 9, the intermediate cooling rates in TFF and SFL offer a means to produce high surface area submicron particles as opposed to lyophilization, with smaller amounts of protein adsorption at gas–liquid interfaces compared to SFD resulting in higher protein stability.

Minimizing gas–liquid interface can improve protein stability by limiting the amount of protein that can adsorb to the interface. For surface active radiolabeled proteins, the surface excess concentration, Γ, (72,73) at full saturation for β-casein, lysozyme, and BSA were 2.6, 3.0, and 3.3 mg/m^2,

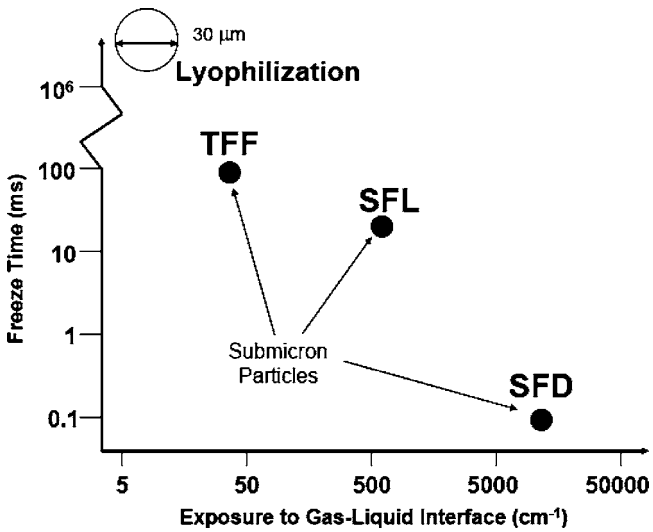

Fig. 9. Freezing time *versus* exposure to gas–liquid interface for lyophilization, thin film freezing (*TFF*), spray freezing into liquid (*SFL*), and spray freeze-drying (*SFD*).

respectively (33,72,73). For LDH, we assumed a similar value of approximately 3 mg/m^2. For the top surface of a 12 mm diameter film, where the surface area is 1.13×10^{-4} m^2, the total adsorbed protein at equilibrium would be 3.4×10^{-4} mg. For a starting 3.6 mm liquid droplet containing 0.25 mg/ml LDH, the total protein is 6.2×10^{-3} mg. Therefore, if all of the protein reached the interface and was denatured, the maximum decrease in protein activity would be 5.5%. The exposure of 1 s may not lead to full equilibrium adsorption. Furthermore, the increase in viscosity as a function of height and time with freezing will arrest diffusion of protein to the air–water interface. For ~10 μm diameter droplets in SFD, it was determined that 25–30% of the total LDH in the droplet adsorbs to the gas–liquid interface in only 0.4 ms (22). Denaturation of part of the adsorbed protein is consistent with the significant decreases in protein activity observed in the SFD process in Table II.

Compared to SFD and SFL, TFF offers the advantage of simplification in the processing steps, in addition to improvement in the stability of the protein. TFF on a cold metal surface bypasses the need to maintain aseptic conditions of a liquid cryogen, for example liquid nitrogen (24). The cooling rate of the thin films in TFF may be controlled readily by varying the temperature of the metal surface. Also, the surface temperature of the film may be measured directly (45). For SFL and SFD, the complex geometry of the turbulent spray in the liquid nitrogen (LN2) combined with the Leidenfrost effect can be somewhat difficult to control and monitor (36). In TFF, more concentrated and thus more viscous solutions may be processed, as the droplets are not atomized. However, the thickness profile of the film along the radius of the frozen disk may change with viscosity. In TFF, collection of the frozen films leads to nearly 100% yields. However, in SFD process yields were only about 80% as the result of entrainment of uncaptured particles in the atomized aqueous stream, particles sticking to the sides of collection vessels, and inefficient separation of the cryogen from the 10–100 μm frozen particles (11,21). TFF is a simple, efficient and robust process for freezing either small (<1 ml) quantities of protein solution or commercial quantities, by freezing droplets in parallel.

CONCLUSIONS

The TFF process was utilized to produce 300 nm lysozyme particles with surface areas on the order of 31–73 m^2/g and 100% LDH activities. Despite a cooling rate of ~10^2 K/s in TFF, the particle sizes and surface areas were similar to those observed in the widely reported process, spray freeze drying SFD, where cooling rates reach 10^6 K/s. In TFF, the thin liquid channels between the ice domains were sufficiently thin and freezing rates of the thin channels sufficiently fast to achieve the similar particle morphologies. Therefore, the extremely rapid cooling rate in the SFD process was not necessary to form the desired submicron protein particles. Although LDH was exposed to the gas–liquid interface of the thin film for a maximum of ~1 s in TFF, the surface area/volume of 45 cm^{-1} was sufficiently small that adsorption produced neglible aggregation and denaturation. Even if this gas–liquid interface became saturated with protein, followed by irreversible denaturation, the maximum activity loss for a 0.25 mg/ml LDH formulation would be 5%. For SFD with a droplet size of 10 μm, the maximum loss could reach 25% in just 0.4 ms from diffusion to the interface and adsorption (22), consistent with the significant decrease in enzyme activity (80%). In SFD, losses in protein stability have been observed in several previous studies (1,11,18,19,21). Although LDH stabilities are high in conventional lyophilization, cooling rates are on the order of 1 K/min resulting in large 30 to 100 μm sized particles (21). Thus, the intermediate cooling rate regime for TFF (and likewise for SFL), relative to SFD and lyophilization, offers a promising route to form stable submicron protein particles of interest in pulmonary and parenteral delivery applications.

ACKNOWLEDGEMENT

This material is supported in part by the STC Program of the National Science Foundation under Agreement No. CHE987664, the Robert A. Welch Foundation, and the Process Science and Technology Center at the University of

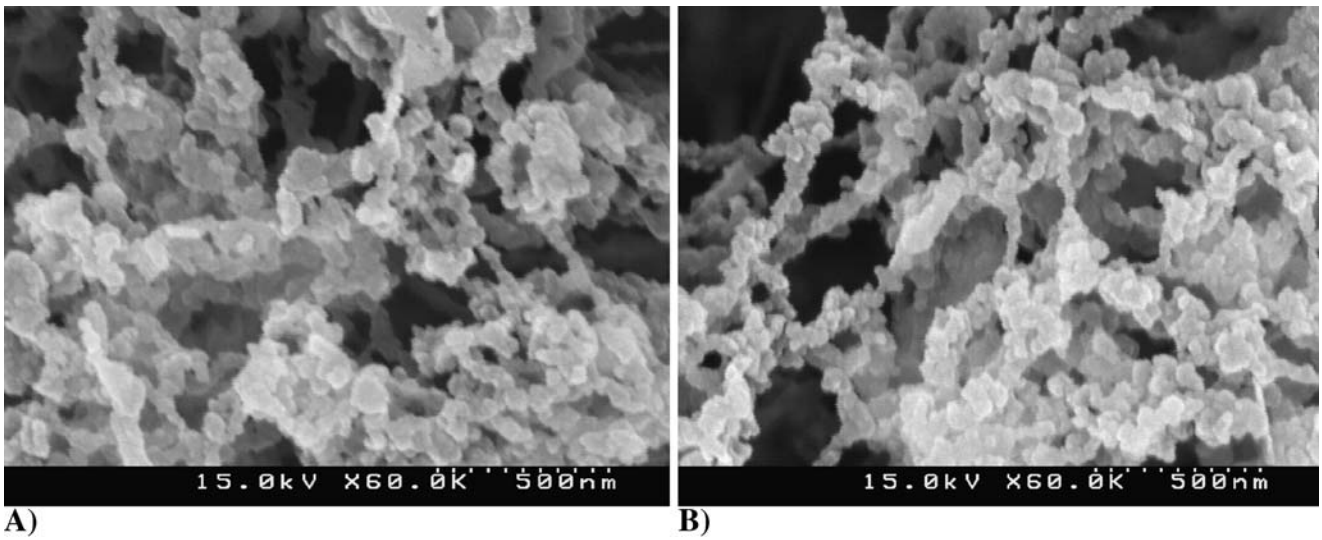

Fig. 10. SEM of top of dried lysozyme thin film at the center (**A**) and approximately 10 μm from the edge (**B**) prepared from a 5 mg/ml lysozyme solution frozen and dried by lyophilization as a thin film on an SEM stage.

Texas. The authors also thank Ted Randolph for highly useful suggestions in the design of this project.

APPENDIX

Supplemental Section

Observed Cooling Patterns of Thin Films

The radial cooling pattern of the thin film on the 223 K surface in Fig. 2, as described further in Fig. 3, indicates that the edge of the film may have been thinner than the center and thus cooled more quickly. Alternatively, previous studies have determined experimentally and theoretically that the edge of a spreading droplet cools at a greater rate than the center even when the thin film deforms into a cylinder (42,56). To understand how the cooling rate difference across the top of the cooling thin film affects the powder morphology, a thin aqueous film containing lysozyme was frozen on an SEM stage and was then dried by lyophilization. The morphology of the top of the dried lysozyme film as observed by SEM (Fig. 10) was uniform across the diameter of the film and had morphological features identical to Fig. 5. Therefore, the small cooling rate difference at the edge of the film *versus* the center had a negligible effect on the dried particle morphology. Thus it is reasonable to model the cooling in the z direction only.

As shown in a previous study, the droplet spreading may terminate as the edge freezes (42). Furthermore, freezing may occur simultaneously with droplet spreading (44). For molybdenum thin films, this edge freezing produced patterns with jagged edges (44), as was also observed in this study at 133 K. The jagged edge indicates fingers of liquid water spread outwards between islands of frozen edges. For a warmer surface (T of 223 K), the edge spread evenly to form a circle without frozen islands, which otherwise would have produced jagged edges. In this case, the radial cooling front moves from the edge of the film to the center (42,56) as was observed experimentally in this study (Fig. 2).

REFERENCES

1. Y.-F. Maa and H. R. Costantino. Spray freeze-drying of biopharmaceuticals: applications and stability considerations. In H. R. Costantino and M. J. Pikal (eds.), *Biotechnology: Pharmaceutical Aspects. 2. Lyophilization of Biopharmaceuticals*, American Association of Pharmaceutical Scientists, Arlington, 2004, pp. 519–561.
2. Y.-F. Maa, L. Zhao, L. G. Payne, and D. Chen. Stabilization of alum-adjuvanted vaccine dry powder formulations: mechanism and application. *J. Pharm. Sci.* **92**:319–332 (2003).
3. X. M. Lam, E. T. Duenas, A. L. Daugherty, N. Levin, and J. L. Cleland. Sustained release of recombinant human insulin-like growth factor-I for treatment of diabetes. *J. Control. Release* **67**:281–292 (2000).
4. W. T. Leach, D. T. Simpson, T. N. Val, E. C. Anuta, Z. Yu, R. O. Williams III, and K. P. Johnston. Uniform encapsulation of stable protein nanoparticles produced by spray freezing for the reduction of burst release. *J. Pharm. Sci.* **94**:56–69 (2005).
5. O. L. Johnson, W. Jaworowicz, J. L. Cleland, L. Bailey, M. Charnis, E. Duenas, C. Wu, D. Shepard, S. Magil, T. Last, A. J. S. Jones, and S. D. Putney. The stabilization and encapsulation of human growth hormone into biodegradable microspheres. *Pharm. Res.* **14**:730–735 (1997).
6. X. M. Lam, E. T. Duenas, and J. L. Cleland. Encapsulation and stabilization of nerve growth factor into poly(lactic-co-glycolic) acid microspheres. *J. Pharm. Sci.* **90**:1356–1365 (2001).
7. M. R. Prausnitz. Microneedles for transdermal drug delivery. *Adv. Drug Deliv. Rev.* **56**:581–587 (2004).
8. D. A. Edwards, J. Hanes, G. Caponetti, J. Hrkach, A. Ben-Jebria, M. L. Eskew, J. Mintzes, D. Deaver, N. Lotan, and R. Langer. Large porous particles for pulmonary drug delivery. *Science* **276**:1868–1871 (1997).
9. S. J. Shire, Z. Shahrokh, and J. Liu. Challenges in the development of high protein concentration formulations. *J. Pharm. Sci.* **93**:1390–1402 (2004).
10. J. L. Cleland, E. T. Duenas, A. Park, A. Daugherty, J. Kahn, J. Kowalski, and A. Cuthbertson. Development of poly-(d,l-lactide-co-glycolide) microsphere formulations containing recombinant human vascular endothelial growth factor to promote local angiogenesis. *J. Control. Release* **72**:13–24 (2001).
11. X. C. Nguyen, J. D. Herberger, and P. A. Burke. Protein powders for encapsulation: a comparison of spray-freeze drying and spray drying of darbepoetin alfa. *Pharm. Res.* **21**:507–514 (2004).
12. S. L. Lee, A. E. Hafeman, P. G. Debenedetti, B. A. Pethica, and D. J. Moore. Solid-State Stabilization of a-Chymotrypsin and Catalase with Carbohydrates. *Ind. Eng. Chem. Res.* **45**:5134–5147 (2006).
13. J. F. Carpenter, B. S. Chang, W. Garzon-Rodriguez, and T. W. Randolph. Rational design of stable lyophilized protein formulations: theory and practice. In J. F. Carpenter and M. C. Manning (eds.), *Pharmaceutical Biotechnology. 13. Rational Design of Stable Protein Formulations*, Kluwer Academic/Plenum Press, New York, 2002, pp. 109–133.
14. M. C. Manning, K. Patel, and R. T. Borchardt. Stability of protein pharmaceuticals. *Pharm. Res.* **6**:903–918 (1989).
15. W. Wang. Lyophilization and development of solid protein pharmaceuticals. *Int. J. Pharm.* **203**:1–60 (2000).
16. R. A. DePaz, D. A. Dale, C. C. Barnett, J. F. Carpenter, A. L. Gaertner, and T. W. Randolph. Effects of drying methods and additives on the structure, function, and storage stability of subtilisin: role of protein conformation and molecular mobility. *Enzyme Microb. Technol.* **31**:765–774 (2002).
17. M. J. Pikal. Mechanisms of protein stabilization during freeze-drying and storage: the relative importance of thermodynamic stabilization and glassy state relaxation dynamics. *Drugs Pharm. Sci.* **137**:63–107 (2004).
18. H. R. Costantino, L. Firouzabadian, K. Hogeland, C. C. Wu, C. Beganski, K. G. Carrasquillo, M. Cordova, K. Griebenow, S. E. Zale, and M. A. Tracy. Protein spray-freeze drying. Effect of atomization conditions on particle size and stability. *Pharm. Res.* **17**:1374–1383 (2000).
19. S. D. Webb, S. L. Golledge, J. L. Cleland, J. F. Carpenter, and T. W. Randolph. Surface adsorption of recombinant human interferon-g in lyophilized and spray-lyophilized formulations. *J. Pharm. Sci.* **91**:1474–1487 (2002).
20. B. S. Chang, B. S. Kendrick, and J. F. Carpenter. Surface-induced denaturation of proteins during freezing and its inhibition by surfactants. *J. Pharm. Sci.* **85**:1325–1330 (1996).
21. Y.-F. Maa and S. J. Prestrelski. Biopharmaceutical powders: particle formation and formulation considerations. *Curr. Pharm. Biotechnol.* **1**:283–302 (2000).
22. M. Adler and G. Lee. Stability and surface activity of lactate dehydrogenase in spray-dried trehalose. *J. Pharm. Sci.* **88**:199–208 (1999).
23. J. Deng, D. R. Davies, G. Wisedchaisri, M. Wu, W. G. J. Hol, and C. Mehlin. An improved protocol for rapid freezing of protein samples for long-term storage. *Acta Crystallogr., Sect. D: Biol. Crystallogr.* **D60**:203–204 (2004).
24. Y. Yamagata, T. Doen, N. Asakawa, and S. Takada. Process for producing protein powder. United States Patent. 6,723,347 (2004).
25. Y.-F. Maa, P.-A. Nguyen, T. Sweeney, S. J. Shire, and C. C. Hsu. Protein inhalation powders: spray drying *vs* spray freeze drying. *Pharm. Res.* **16**:249–254 (1999).
26. S. P. Sellers, G. S. Clark, R. E. Sievers, and J. F. Carpenter. Dry powders of stable protein formulations from aqueous solutions

prepared using supercritical CO(2)-assisted aerosolization. *J. Pharm. Sci.* **90**:785–797 (2001).
27. J. D. Andya, Y.-F. Maa, H. R. Costantino, P.-A. Nguyen, N. Dasovich, T. D. Sweeney, C. C. Hsu, and S. J. Shire. The effect of formulation excipients on protein stability and aerosol performance of spray-dried powders of a recombinant humanized anti-IgE monoclonal antibody. *Pharm. Res.* **16**:350–358 (1999).
28. Y.-F. Maa and P.-A. Nguyen. Method of spray freeze drying proteins for pharmaceutical administration. United States Patent. 6,284,282 (2001).
29. H. R. Costantino, L. Firouzabadian, C. C. Wu, K. G. Carrasquillo, K. Griebenow, S. E. Zale, and M. A. Tracy. Protein spray freeze drying. 2. Effect of formulation variables on particle size and stability. *J. Pharm. Sci.* **91**:388–395 (2002).
30. Z. H. Chang and J. G. Baust. Ultra-rapid freezing by spraying/plunging: pre-cooling in the cold gaseous layer. *J. Microsc.* **161**:435–444 (1991).
31. Z. Yu, K. P. Johnston, and R. O. Williams III. Spray freezing into liquid *versus* spray-freeze drying: Influence of atomization on protein aggregation and biological activity. *Eur. J. Pharm. Sci.* **27**:9–18 (2006).
32. J. D. Engstrom, D. T. Simpson, C. Cloonan, E. Lai, R. O. Williams III, G. B. Kitto, and P. Johnston Keith. Stable high surface area lactate dehydrogenase particles produced by spray freezing into liquid nitrogen. *Eur. J. Pharm. Biopharm.* **65**:163–174 (2007).
33. S. Magdassi and A. Kamyshny. Surface activity and functional properties of proteins. In S. Magdassi (ed.), *Surface Activity of Proteins*, Marcel Dekker, New York, 1996, pp. 1–38.
34. Z. Yu, A. S. Garcia, K. P. Johnston, and R. O. Williams III. Spray freezing into liquid nitrogen for highly stable protein nanostructured microparticles. *Eur. J. Pharm. Biopharm.* **58**:529–537 (2004).
35. Z. Yu, T. L. Rogers, J. Hu, K. P. Johnston, and R. O. Williams III. Preparation and characterization of microparticles containing peptide produced by a novel process: spray freezing into liquid. *Eur. J. Pharm. Biopharm.* **54**:221–228 (2002).
36. J. D. Engstrom, D. T. Simpson, E. Lai, R. O. Williams III, and K. P. Johnston. Morphology of protein particles produced by spray freezing of concentrated solutions. *Eur. J. Pharm. Biopharm.* **65**:149–162 (2007).
37. H. Sitte, L. Edelmann, and K. Neumann. Cryofixation without pretreatment at ambient pressure. In R. A. Steinbrecht and K. Zierold (eds.), *Cryotechniques in Biological Electron Microscopy*, Springer-Verlag, Berlin, 1987, pp. 87–113.
38. J. C. Gilkey and L. A. Staehelin. Advances in ultrarapid freezing for the preservation of cellular ultrastructure. *J. Electron Microsc. Tech.* **3**:177–210 (1986).
39. J. A. N. Zasadzinski. A new heat transfer model to predict cooling rates for rapid freezing fixation. *J. Microsc.* **150**:137–149 (1988).
40. J. E. Heuser, T. S. Reese, and D. M. Landis. Preservation of synaptic structure by rapid freezing. *Cold Spring Harbor Symp. Quant. Biol.* **40**:17–24 (1976).
41. J. Escaig. New instruments which facilitate rapid freezing at 83 K and 6 K. *J. Microsc.* **126**:221–230 (1982).
42. J. Fukai, T. Ozaki, H. Asami, and O. Miyatake. Numerical simulation of liquid droplet solidification on substrates. *J. Chem. Eng. Jpn.* **33**:630–637 (2000).
43. T. Bennett and D. Poulikakos. Splat-quench solidification: estimating the maximum spreading of a droplet impacting a solid surface. *J. Mater. Sci.* **28**:963–970 (1993).
44. H. Zhang, X. Y. Wang, L. L. Zheng, and X. Y. Jiang. Studies of splat morphology and rapid solidification during thermal spraying. *Int. J. Heat Mass Transfer* **44**:4579–4592 (2001).
45. K. A. Overhoff, J. D. Engstrom, B. Chen, T. L. Rogers, K. P. Johnston, and R. O. Williams III. Development and optimization of the novel ultra-rapid freezing particle engineering process to enhance the dissolution rates of poorly water soluble drugs. *Eur. J. Pharm. Biopharm.* **65**:57–67 (2007).
46. J. Fukai, M. Tanaka, and O. Miyatake. Maximum spreading of liquid droplets colliding with flat surfaces. *J. Chem. Eng. Jpn.* **31**:456–461 (1998).
47. M. Pasandideh-Fard, R. Bhola, S. Chandra, and J. Mostaghimi. Deposition of tin droplets on a steel plate: simulations and experiments. *Int. J. Heat Mass Transfer* **41**:2929–2945 (1998).
48. M. Pasandideh-Fard, S. Chandra, and J. Mostaghimi. A three-dimensional model of droplet impact and solidification. *Int. J. Heat Mass Transfer* **45**:2229–2242 (2002).
49. D. Sivakumar and H. Nishiyama. Numerical analysis on the impact behavior of molten metal droplets using a modified splat-quench solidification model. *J. Heat Transf.-Trans. ASME* **126**:1014–1022 (2004).
50. B. Kang, Z. Zhao, and D. Poulikakos. Solidification of liquid metal droplets impacting sequentially on a solid surface. *J. Heat Transfer* **116**:436–445 (1994).
51. J. Madejski. Solidification of droplets on a cold surface. *Int. J. Heat Mass Transfer* **19**:1009–1013 (1976).
52. C. S. Marchi, H. Liu, E. J. Lavernia, R. H. Rangel, A. Sickinger, and E. Muehlberger. Numerical analysis of the deformation and solidification of a single droplet impinging onto a flat substrate. *J. Mater. Sci.* **28**:3313–21 (1993).
53. G. X. Wang and E. F. Matthys. Modeling of heat transfer and solidification during splat cooling: effect of splat thickness and splat/substrate thermal contact. *Int. J. Rapid Solid* **6**:141–74 (1991).
54. G. X. Wang and E. F. Matthys. Numerical modeling of phase change and heat transfer during rapid solidification processes: use of control volume integrals with element subdivision. *Int. J. Heat Mass Transfer* **35**:141–53 (1992).
55. Z. Zhao, D. Poulikakos, and J. Fukai. Heat transfer and fluid dynamics during the collision of a liquid droplet on a substrate. I. Modeling. *Int. J. Heat Mass Transfer* **39**:2771–2789 (1996).
56. Z. Zhao, D. Poulikakos, and J. Fukai. Heat transfer and fluid dynamics during the collision of a liquid droplet on a substrate. II. Experiments. *Int. J. Heat Mass Transfer* **39**:2791–2802 (1996).
57. G. Trapaga and J. Szekely. Mathematical modeling of the isothermal impingement of liquid droplets in spraying processes. *Metall. Trans. B.* **22B**:901–14 (1991).
58. T. J. Anchordoquy and J. F. Carpenter. Polymers protect lactate dehydrogenase during freeze-drying by inhibiting dissociation in the frozen state. *Arch. Biochem. Biophys.* **332**:231–238 (1996).
59. T. J. Anchordoquy, K.-I. Izutsu, T. W. Randolph, and J. F. Carpenter. Maintenance of quaternary structure in the frozen state stabilizes lactate dehydrogenase during freeze-drying. *Arch. Biochem. Biophys.* **390**:35–41 (2001).
60. S. Brunauer, P. H. Emmett, and E. Teller. Adsorption of gases in multimolecular layers. *J. Am. Chem. Soc.* **60**:309–319 (1938).
61. E. H. Snell, R. A. Judge, M. Larson, and M. J. van der Woerd. Seeing the heat—preliminary studies of cryocrystallography using infrared imaging. *J. Synch. Radiat.* **9**:361–367 (2002).
62. A. A. Elkordy, R. T. Forbes, and B. W. Barry. Integrity of crystalline lysozyme exceeds that of a spray-dried form. *Int. J. Pharm.* **247**:79–90 (2002).
63. J. Fukai, Y. Shiiba, T. Yamamoto, O. Miyatake, D. Poulikakos, C. M. Megaridis, and Z. Zhao. Wetting effects on the spreading of a liquid droplet colliding with a flat surface—experiment and modeling. *Phys. Fluids* **7**:236–247 (1995).
64. S. Schiaffino and A. A. Sonin. Motion and arrest of a molten contact line on a cold surface: an experimental study. *Phys. Fluids* **9**:2217–2226 (1997).
65. T. Bennett and D. Poulikakos. Heat-Transfer Aspects of Splat-Quench Solidification—Modeling and Experiment. *J. Mater. Sci.* **29**:2025–2039 (1994).
66. H. S. Carslaw and J. C. Jaeger. Conduction of Heat in Solids. Oxford University Press, London, 1959.
67. F. Franks. Biophysics and Biochemistry at Low Temperatures. Cambridge University Press, New York, 1985.
68. P. G. Debenedetti. Supercooled and glassy water. *J. Phys.: Condens. Matter* **15**:R1669–R1726 (2003).
69. E. Mayer and P. Brueggeller. Vitrification of pure liquid water by high pressure jet freezing. *Nature* **298**:715–718 (1982).
70. C. A. Angell. Liquid fragility and the glass transition in water and aqueous solutions. *Chem. Rev.* **102**:2627–2649 (2002).
71. C. A. Angell and L.-M. Wang. Hyperquenching and cold equilibration strategies for the study of liquid–liquid and protein folding transitions. *Biophys. Chem.* **105**:621–637 (2003).
72. D. E. Graham and M. C. Phillips. Proteins at liquid interfaces. I. Kinetics of adsorption and surface denaturation. *J. Colloid Interface Sci.* **70**:403–414 (1979).
73. D. E. Graham and M. C. Phillips. Proteins at liquid interfaces. II. Adsorption Isotherms. *J. Colloid Interface Sci.* **70**:415–426 (1979).